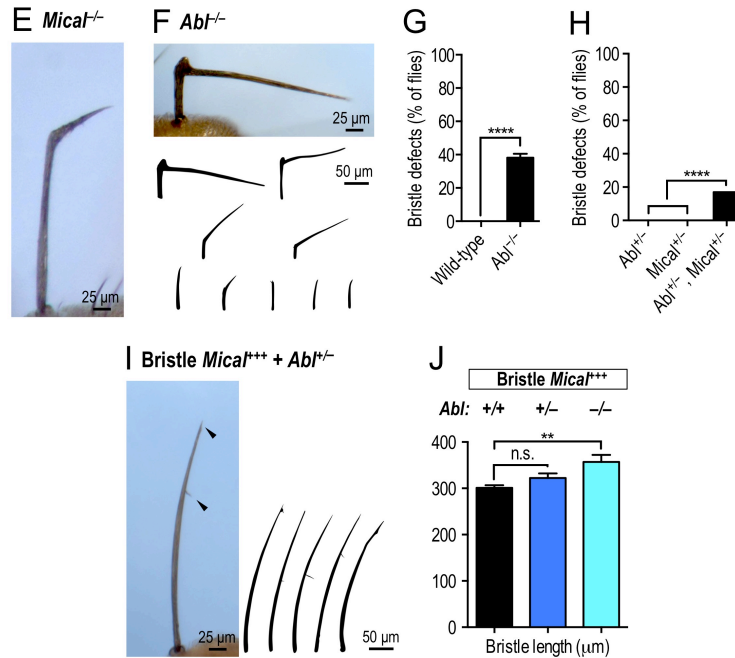
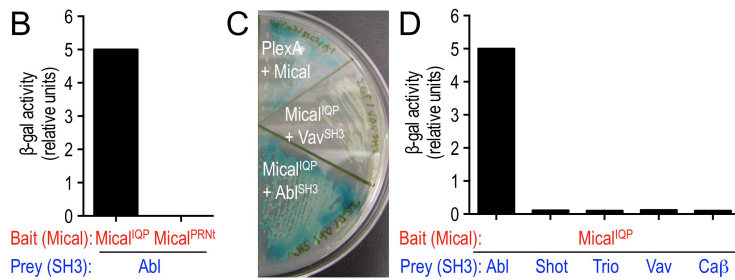


## A PxxP motifs in Mical

FRLR**PKPL**PQRTNKAARKSAAAQ**PASPAV**PTAGSVPTAAATSEHMDTTPPRDQVLLQTSRANASADAMSDEANVIDEH  
 EWSGRNFLPESNNDSQSELSSSDESDESSEMFEEDDSPFGAQTLLQASDWIGKYCEDSDSDDFYDSSEGIADDDGK  
 DDTEGEEFKARELRRQEVRLQPLPANLPTDTETEVTQTESESTSPDEVELNSATEISTDSEFDNDEIIRQAPKIFIDDTH  
 LRKPTKVIKSTMIIPNAASAGLHQKQLAAREKGGSYLQYQ**QPP**LSQFKPLVQVDPDLLIGSQRAPLQNPDPGYLLN  
 KTASTEGIASKSLLELKKRYLLGEPANGDKIQKSGSTSVLDSRIRSFQSNISECQKLLNPSDDISAGMRTFLDRTKLGG  
 SQTTPGQTNELIRSATSNVINDLRVELRIQKTDSSHSTDNENKENVFNCKNELNKGMEYTDVAVNATLLDQLARKSS**PTTP**  
 TNKTVVVEIDLVT**PEKPI**IDIIDLTALETPKKQLVDGSAMDVDERLTPDSNKISELQQEVKEEPPKPDVSRDVKECIPDILG  
 HIKEGTGSKPEGGEDQOSSLLEQSDDEEKRDSPKDVAEHELVEPDSVQIQV**PNIP**WEKSKPEVMSTGGSGSICSSSDSS  
 IEDIQHYILESTTSPDTQTVGGKHNVPRLEVHDTSGALMVDLSLMIVNGKYIGDPEDVKFLDMPANVIV**PAP**ALKTNEL  
 DMEDDQEAEEAPVTATPEPVECTVIEAERRVTAP**PPL**PEMGPPKLFKDSKNENKIESLKNLPLIVESNVEHSQAVKPIITL  
 NLSNLRAT**PDTPTT**TAHDSDKTPTGEILSRGSDSETEHTGTGQVLTETELSDWTADDCISENFVDLEFALNSNKGITKR  
 RKDRRSKASKLPNGNEVIEHELARQAPVVQMDGILLSAIDIDDIEMDTGSEGSCEAEYPATNTALIQRNGYMEYIEAEPK  
 KTRRKAAPPSSYPGNLPLMTKRDEKLGVDYIEQGAYIMHDDAKTPVNEVAPAMTQSLTDSITLNELDDDSMIISQTPT  
 TTESEALTVVTSPLDTSRPRVLDQFASMLAAGKGDSTPSSSEQPKTSTVTSSTGPNSSSTGTVNSKEPQEEELQIQFE  
 VYRALQQRISQISTQRKSSKGEAPNLQLNSSAPVIESAED**PAK**AEELVSMRPTTISGKV**PEIPT**LSSKLEETKE  
 RTKQKDLIHDLVMDKLSKQKQLNAEKRLHRSRQSLTSGYASGSSLSPTKLAACSPQDSNCSQAHYHASTAEAE**PK**  
**PA**ERPLQKSATSTYVSPYRTVQAPTRSDLYKPRPFSEHIDSNALAGYKLGKTASFNQKLGDFAK**IAPAR**VNRGGGV  
 ATADIANISASTENLRSEARARARLKSNTLGLSPEEKMLIRSLRHYDQNRSLKPKQLEEMPGLAARARKMSASKV  
 NDLAYMVGQQQQQVEKDAVLQAKAADFTSDPNLASGGQEKAGRTKSGRR**PKDPER**RKSLIQLSLSPFKQKSGSAASSK  
 EQGGVAVAHVHSEQSERPGTSSSGTPTISDAAGGGGGGGVFRFRISPKSKEKSKSCFDLRFNFGDKMLVCNAASAPG  
 ATSAQKNHSQEYLNLTNNSRYRKQNTAKPKPEFSSSSPQLYIHKPHHLLAAHPSALDDQT**PPP****IPPL**PLNYQRSDDE  
 SYANETREH



**Figure S1. Further analyses of the association between Mical and Abl. Related to Figure 1.** (A) Drosophila Mical, similar to mammalian MICALS, includes a long-proline rich region containing multiple PxxP motifs (marked in red) (Terman, et al., 2002), which are known interacting partners with SH3 domains. (B-D) A particular portion of the proline-rich region of Mical specifically interacts with the SH3 domain of the Abl tyrosine kinase. (B) The SH3 domain of Abl tyrosine kinase specifically interacts with the C-terminal part of the Mical proline-rich region (the Mical<sup>IQP</sup> region, amino acids 1951-2550). No interactions were observed between the Abl<sup>SH3</sup> and the other part of Mical proline-rich region (the Mical<sup>PRNt</sup> region, amino acids 861-1539). (C) A representative image of a yeast two-hybrid interaction assay. The interaction between PlexA and Mical was used as a positive control (Terman, et al., 2002). Note the strong blue color indicative of  $\beta$ -gal activity of the yeast expressing both the Abl<sup>SH3</sup> and the Mical<sup>IQP</sup>. The yeast expressing the SH3 domain of Vav and Mical<sup>IQP</sup> did not exhibit the same blue color. (D) The Mical<sup>IQP</sup> shows the hallmarks of specifically interacting with the Abl<sup>SH3</sup>. The SH3 domains of other proteins including Shot, Trio, Vav, and the calcium channel  $\beta$  subunit do not exhibit the hallmarks of a yeast interaction with Mical<sup>IQP</sup> (as the slight blue color was similar to the background color that this bait

alone exhibits after several days of growth [data not shown]). The interactions were measured by beta-galactosidase ( $\beta$ -gal) activity both in B and D. **(E-H)** *Abl* mutants have similar bristle defects and genetically interact with *Mical* mutants. **(E)** *Mical* mutant bristles are straight, thick, and/or bent (see also (Hung, et al., 2013; Hung, et al., 2010)). **(F-G)** *Abl* homozygous viable mutant ( $Abl^2/Abl^4$ ) bristles resemble *Mical* loss-of-function mutant bristles and are straight and/or bent (as shown in F). The weaker  $Abl^2/Abl^4$  mutant allele was used because adults survived into adulthood and therefore could be scored for bristle defects – and the percentage of adult flies containing bristle defects in *wild-type* and *Abl* mutant ( $Abl^2/Abl^4$ ) flies are shown in G.  $n \geq 40$  adults/genotype; mean  $\pm$  s.e.m.; t-test; \*\*\*\*P  $\leq 0.0001$ .  $Abl^{-/-} = Abl^2/Abl^4$ . **(H)** Compared to *Abl* heterozygous mutants ( $Abl^4/+$ ) or *Mical* heterozygous mutants ( $Mical^{Df(3R)Swp2}/+$ ) alone, *Abl/Mical* transheterozygous mutants ( $Abl^4/+$ ,  $Mical^{Df(3R)Swp2}/+$ ) have bristle defects, indicating a genetic interaction between the two loss-of-function alleles.  $n \geq 30$  adults/genotype;  $X^2$  test; \*\*\*\*P  $\leq 0.0001$ . Similar genetic interactions with *Abl* were also tested and seen with  $Mical^{K1496}/+$  and  $Mical^{I696}/+$ . **(I-J)** Decreasing the levels of *Abl* suppresses *Mical*-mediated F-actin alterations/cellular remodeling. **(I)** Decreasing the levels of *Abl* (*Abl* heterozygous mutant [ $Abl^{+/-}$ ] background) suppresses *Mical*-mediated F-actin alterations/bristle branching. See also data from these experiments in **Figure II**.  $Abl^{+/-} = Abl^4/+$ . Similar interactions were also tested and seen with  $Abl^1/+$ ,  $Abl^2/+$ ,  $Abl^4/+$ . **(J)** Quantification of adult bristle length (main shaft length) following genetic manipulations of *Mical* and *Abl*.  $n \geq 7$  bristles/genotype; mean  $\pm$  s.e.m.; t-test; \*\*P  $\leq 0.01$ ; n.s. not significant.  $Abl^{+/-} = Abl^4/+$ . Similar interactions were also tested and seen with  $Abl^1/+$ ,  $Abl^2/+$ ,  $Abl^4/+$ .

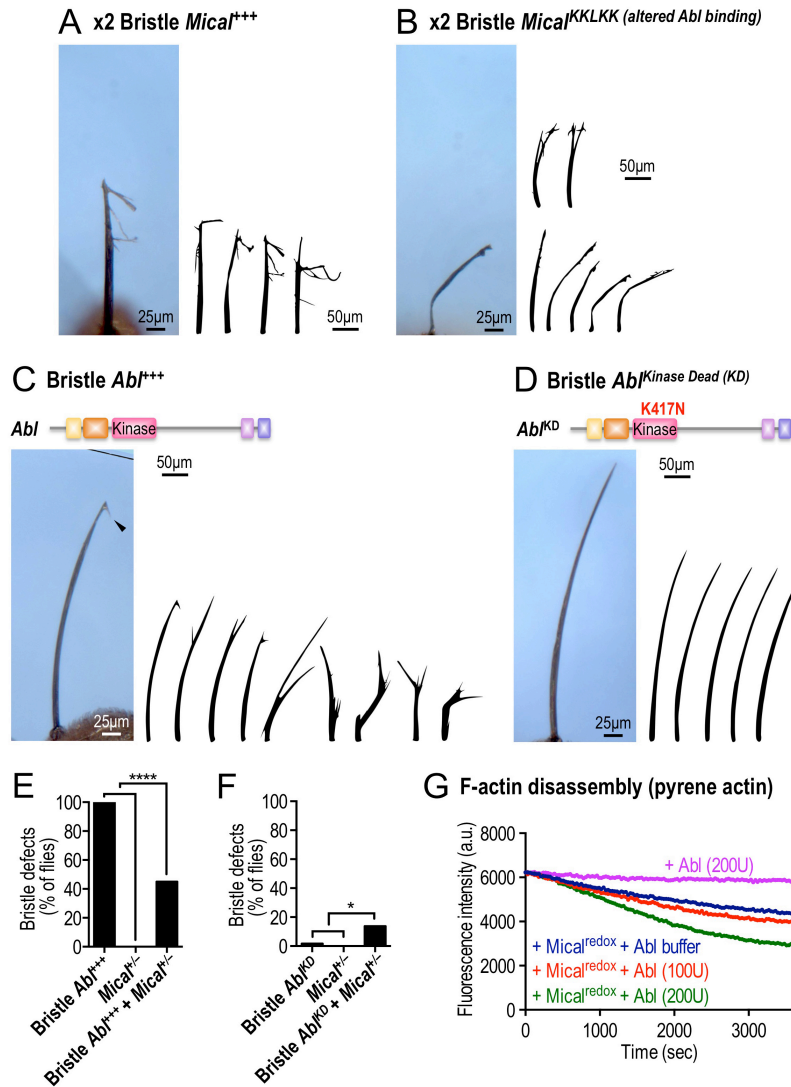



**Figure S2. Further analysis of Abl kinase mediated effects on Mical's actin regulatory activity. Related to Figures 1 and 2.** (A-B) Bristle expression of high levels (2 copies) of *Mical*<sup>KLLKK</sup> generates morphological defects suggestive of it functioning in a dominant negative manner. (A) Bristle specific expression of high levels (2 copies) of wild-type *Mical* further increases F-actin alterations/bristle branching (compare to **Figure 1F** expressing one copy of wild-type *Mical*; see also (Hung, et al., 2010)). (B) In contrast, bristle specific expression of high levels (2 copies) of *Mical*<sup>KLLKK</sup> generates bristle defects that are qualitatively different than those we observed following similar increases in wild-type *Mical* (A) and included bristle bends that resembled those defects seen following expression of dominant negative forms of Mical (Hung, et al., 2010). These results also indicate that the suppression of Mical-mediated branching by *Mical*<sup>KLLKK</sup> is not caused by insufficient expression levels of *Mical*<sup>KLLKK</sup> protein. (C) Expression of an *Abl* transgene alone in bristles (Bristle *Abl*<sup>+/+</sup>) induces F-actin reorganization/cellular remodeling. These effects range from the formation of a single branch (image and drawings on the left [when one copy of *Abl* is expressed in bristles]) to numerous branches and dramatically shortened bristles (drawings on the right [when two copies of *Abl* are expressed in bristles]). These data are quantified in **Figures 2C** and **S2E** for bristle expression of one copy of *Abl*. (D) Expression of *Abl*<sup>KD</sup>, unlike wild-type *Abl* (compare with **Figure S2C**), does not alter bristle morphology indicating that an intact Abl kinase domain is required for Abl-mediated bristle remodeling. This data is quantified in **Figure 2C** for bristle expression of one copy of *Abl*<sup>KD</sup>. (E-F) Genetic interactions between *Abl* and *Mical* demonstrate functions in Abl-mediated F-actin/cellular remodeling. (E) Decreasing the levels of *Mical* (*Mical*<sup>+/-</sup> [heterozygous mutant]) suppresses Abl-mediated bristle branching indicating that Mical is required for Abl-mediated F-actin/cellular remodeling. n ≥ 29 adults/genotype (all bristles (macrochaetae) examined);  $\chi^2$  test; \*\*\*\*P ≤ 0.0001. *Mical*<sup>+/-</sup> = *Mical*<sup>Df(3R)Swp2/+</sup>. (F) Decreasing *Mical* levels (*Mical*<sup>+/-</sup> [heterozygous mutant]) in combination with bristle specific expression of a kinase-dead Abl (*Abl*<sup>KD</sup>) induces bristle defects that resemble both *Mical* and *Abl* loss-of-function (knockout) mutants (i.e., bent bristles; see **Figures S1E and S1F**). These results also indicate that *Abl*<sup>KD</sup> functions as a dominant negative inhibitor of wild-type Abl. n ≥ 58 adults flies/genotype (all bristles (macrochaetae) examined);  $\chi^2$  test; \*P ≤ 0.05. *Mical*<sup>+/-</sup> = *Mical*<sup>Df(3R)Swp2/+</sup>. (G) Pyrene-labeled actin depolymerization assays as in **Figure 2D**. Actin filaments disassemble (decreasing fluorescence) in the presence of *Mical*<sup>redox</sup> (50 nM) (blue [preincubated with Abl kinase buffer]; see also (Hung, et al., 2010)). Pre-incubation of *Mical*<sup>redox</sup> (50 nM) with the Abl kinase increases the rate and extent of this Mical-mediated actin depolymerization in an Abl kinase concentration dependent manner (compare the effects of 100 U of Abl kinase [red] to 200 U of Abl kinase [green] on *Mical*<sup>redox</sup>-mediated effects). Abl kinase alone does not affect actin depolymerization (pink). Mical's co-enzyme NADPH was present in all conditions.

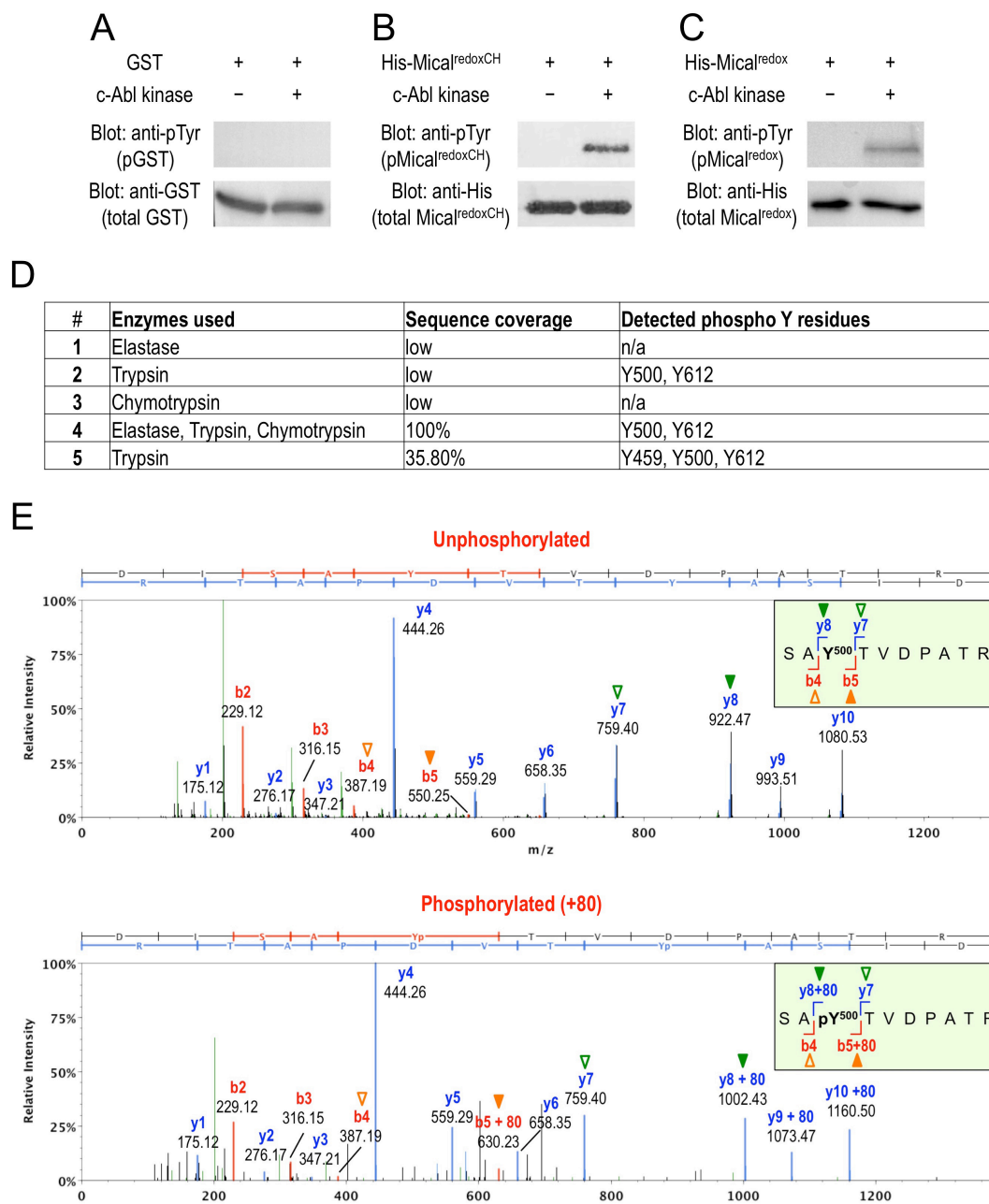


**Figure S3. Abl phosphorylates the Y<sup>500</sup> residue within the redox domain of Mical. Related to Figure 3.** (A-C) Abl specifically phosphorylates purified Mical<sup>redoxCH</sup> (B) and purified Mical<sup>redox</sup> (C) protein but not purified GST protein (A). This phosphorylation was detected using antibodies against phospho-tyrosine residues and gave similar results to those presented in **Figure 3A** and data not shown. (D) Summary of mass spectrometry to analyze phosphorylated Mical<sup>redoxCH</sup> protein. We performed mass measurements on purified Mical<sup>redoxCH</sup> protein, following preincubation with Abl and ATP. Masses of digested peptides of Mical<sup>redoxCH</sup> were measured in five independent experiments/phosphorylation samples/mass analyses (#) using different enzymes or combinations of enzymes (Enzymes used) in two different Mass Spectrometry Labs. Phosphorylation of Y<sup>500</sup> and Y<sup>612</sup> were detected in three of the mass analyses. In the Mical<sup>redoxCH</sup> protein, the Y<sup>500</sup> residue resides in the redox domain and Y<sup>612</sup> residue resides in the CH domain. Between these two sites, only the Y<sup>500</sup> residue is evolutionarily conserved from flies to humans (see **Figure S4A**). Furthermore, only the Y<sup>500</sup> residue is present in the actin-regulatory redox region of Mical, while the Y<sup>612</sup> residue is in the CH domain of Mical, which is a domain that is not required for Mical-mediated F-actin disassembly in vitro (Hung, et al., 2010). Likewise, we found that the CH domain is not required for Abl's ability to phosphorylate Mical (**Figure S3C**) or Abl's ability to regulate Mical-mediated F-actin disassembly (**Figures 2D-2H and S2G**). Thus, our results suggested that Mical's Y<sup>500</sup> residue may be critical for Abl's effect on Mical. (E) Comparison of the mass spectra of the unphosphorylated and phosphorylated peptides reveals a mass increase (+ 80) on Y<sup>500</sup>. In particular, individual amino acid bonds were broken from both ends of the peptide chain (y1-y10, b2-b5) and the mass was determined for the generated fragments. For example, comparing y8 (green closed arrowhead) and y7 (green open arrowhead) fragments between and within samples shows a + 80 mass increase on the y8 ion (Y500). Comparing the b ions (breaking the peptide in the opposite direction, orange arrowheads) also reveals a similar mass increase on Y500.

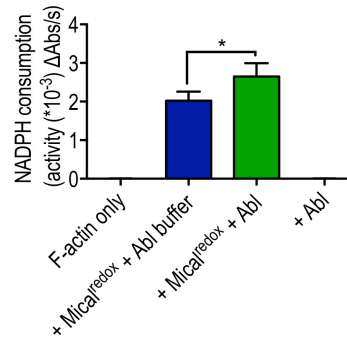


### A Conserved Abl phosphorylation site

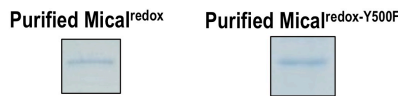


*Dm* Mical 495 RDISA<sup>Y500</sup>TVDPA  
*Hs* MICAL-1 453 RNVAQ<sup>Y458</sup>GLDPA  
*Hs* MICAL-2 458 KNFEQ<sup>Y463</sup>TLDPG  
*Hs* MICAL-3 458 KNFSQ<sup>Y463</sup>SIDPV

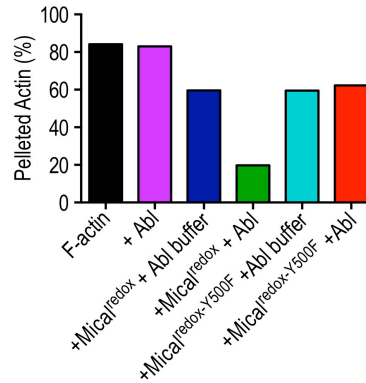
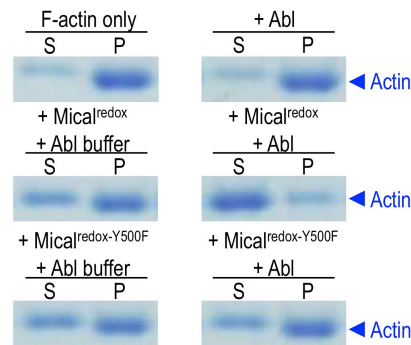
### B Abl increases Mical's enzymatic activity



### C Purified Proteins



### D Abl, Mical<sup>Y500</sup> & F-actin Disassembly



### E x2 Bristle *Mical*<sup>Y500F</sup>

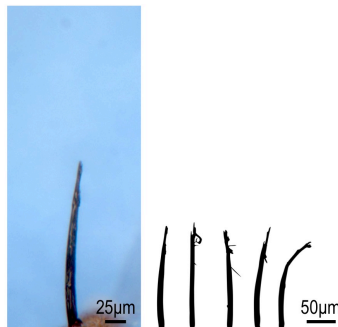


**Figure S4. Further analyses of Abl-mediated phosphorylation of Mical to enhance Mical's Redox enzymatic F-actin disassembly activity. Related to Figure 3.** (A) The Mical Y<sup>500</sup> residue is evolutionarily conserved from flies to mammals, and it is also conserved in all three human MICAL family members (MICAL-1, MICAL-2, and MICAL-3). (B) Additional analysis of the enzyme activity of Mical (following on Figure 3D) supports that the active Abl kinase increases Mical's enzymatic activity (as determined by conversion of Mical's co-enzyme NADPH to NADP<sup>+</sup>). [Mical] = 50 nM, [Abl] = 200 U, [NADPH] = 100 µM, n = 4; mean ± s.e.m.; t-test; \*P ≤ 0.05. (C) Coomassie stained gels show purified Mical<sup>redox</sup> and Mical<sup>redox-Y500F</sup> proteins. (D) Actin sedimentation assays (similar to Figure 2G-2H), using the same experimental strategy described in Figure 2G, also reveal that substitution of Mical's Y<sup>500</sup> residue to F<sup>500</sup> (phenylalanine) abolishes Abl's ability to enhance Mical<sup>redox</sup>-mediated F-actin disassembly. S, supernatant (G-actin); P, pellet (F-actin); n = 2. (E) Bristle specific expression of high levels (2 copies) of *Mical*<sup>Y500F</sup> generates morphological defects that are qualitatively different than the heavily branched bristles we observed following similar increases in wild-type Mical (see Figure S2A; (Hung, et al., 2010)). The bristle alterations resembled those defects seen in *Mical* loss-of-function mutants and following expression of dominant negative forms of Mical (Hung, et al., 2010). These results also indicate that the suppression of Mical-mediated branching by *Mical*<sup>Y500F</sup> is not caused by insufficient expression levels of *Mical*<sup>Y500F</sup> protein.

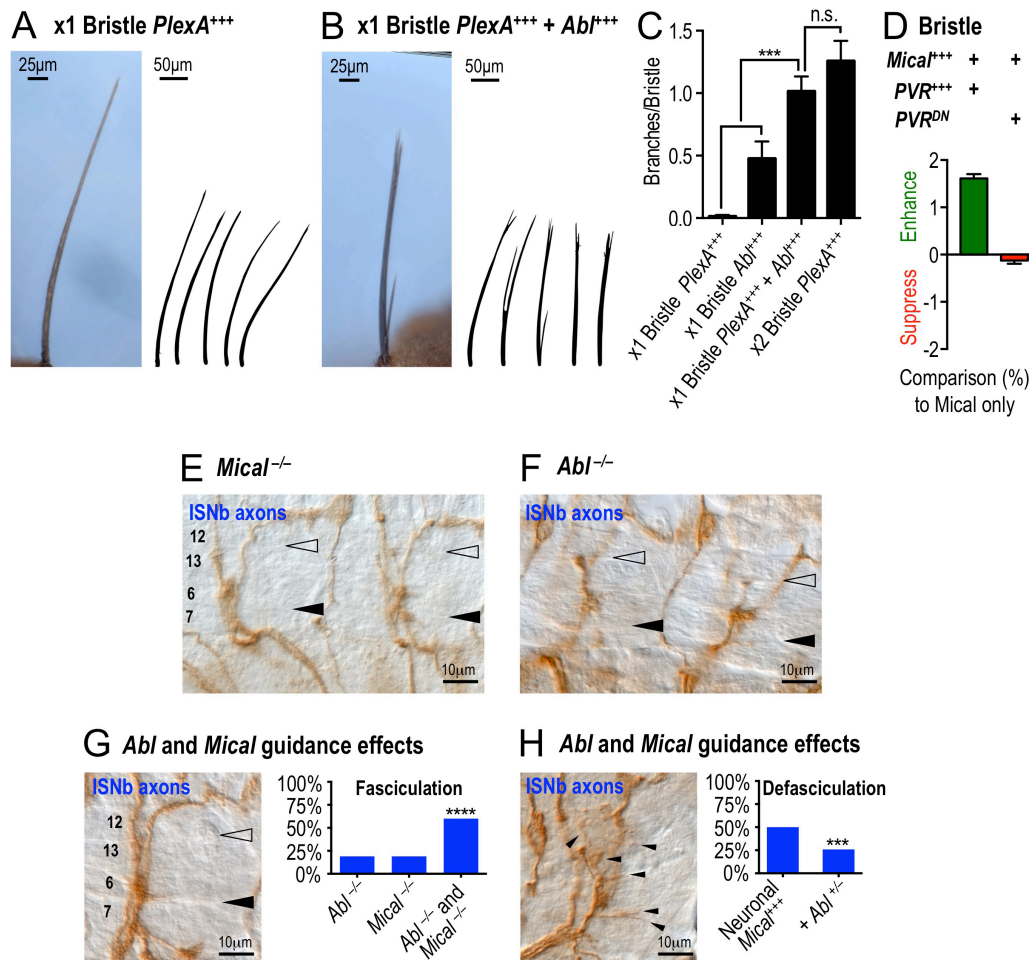


**Figure S5. Further analysis of Semaphorin/Plexin enhancement of Abl and Mical effects and the interactions between Mical and Abl in axon guidance. Related to Figures 4 and 5.** (A-C) Raising the levels of Abl enhances Plexin-mediated F-actin/cellular remodeling. Overexpressing low levels of *PlexA* (x1) specifically in bristles results in limited bristle branching (A, C; see also (Hung, et al., 2010)). Co-expressing x1 *PlexA* in combination with *Abl* in bristles significantly enhances PlexA and Abl-mediated bristle branching and generates bristles that resemble those seen with high-levels (x2) of bristle *PlexA* expression (B-C, also compare to **Figure 4A**).  $n \geq 39$  bristles/genotype; mean  $\pm$  s.e.m.; t-test; \*\*\* $P \leq 0.001$ ; n.s. not significant. (D) Increasing the bristle levels of *PVR* (*PVR*<sup>+++</sup>) enhances Mical-induced (*Mical*<sup>+++</sup>) F-actin alterations/cellular remodeling and generates bristles with longer, and more complex and numerous branches (see also **Figure 4E and 4G**). In contrast, bristle specific expression of a signaling incompetent/dominant negative version of PVR (*PVR*<sup>DN</sup>), which contains only the extracellular domain and transmembrane regions of PVR (Inaki, et al., 2012), suppresses *PVR*'s effects on Mical-induced F-actin alterations/cellular remodeling. These suppressive effects on Mical-mediated F-actin alterations/cellular remodeling were similar to those we observed with the kinase dead version of Abl (*Abl*<sup>KD</sup>) (see **Figure 2B-C**).  $n \geq 24$  bristles/genotype; mean  $\pm$  s.e.m. (E-H) Further analyses of the interaction between Mical and Abl in axon guidance. (E-F) *Mical* and *Abl* mutants exhibit similar axon guidance defects. In particular, both *Mical* and *Abl* are required for normal connectivity of the nervous system and have both been well-defined for their important role in the guidance of axons (reviewed in (Wilson, et al., 2016; Thompson and Van Vactor, 2006; Moresco and Koleske, 2003)). We therefore examined whether *Mical* and *Abl* functionally interact to orchestrate axon guidance. Axons within the *Drosophila* embryonic nervous system exhibit a stereotypic pattern of extension and innervation that provides a model to characterize proteins important for axon guidance. Axons within the intersegmental motor nerve b (ISNb) pathway, for example, are easily observed following their defasciculation from the main intersegmental nerve (ISN) and as they elongate to specifically innervate muscles 6/7 and 12/13 (see also **Figure 5C**). (E) *Mical* repulsive signaling is required for ISNb motor axons to selectively defasciculate from the ISN and innervate muscle 6/7 and 12/13 (Hung, et al., 2013; Hung, et al., 2010; Beuchle, et al., 2007; Terman, et al., 2002), such that in *Mical*<sup>-/-</sup> mutants, ISNb axons fail to defasciculate normally, often stalling along their pathway and exhibiting decreased innervation of their muscle targets. For example, in the image (E) ISNb axons of *Mical* mutants (*Mical*<sup>Df(3R)Swp2</sup>; (Terman, et al., 2002)) exhibit stall/bypass defects and fail to defasciculate and innervate their target muscles 6 and 7 (closed arrowheads) and 12 and 13 (open arrowheads). *Mical*<sup>-/-</sup> = *Mical*<sup>Df(3R)Swp2</sup> and similar phenotypes were seen with other alleles and combinations of alleles (see also (Hung, et al., 2013; Hung, et al., 2010; Beuchle, et al., 2007; Terman, et al., 2002)). (F) Similar to *Mical* mutants, ISNb axons of *Abl* mutants (e.g., *Abl*<sup>2</sup>; (O'Donnell and Bashaw, 2013; Wills, et al., 1999)) exhibit similar ISNb stall/bypass defects and often fail to defasciculate and innervate their target muscles 6 and 7 (closed arrowheads) and 12 and 13 (open arrowheads). *Abl*<sup>-/-</sup> = *Abl*<sup>2</sup> and similar phenotypes were seen with other alleles and combinations of alleles (e.g., and see also (O'Donnell and Bashaw, 2013; Song, et al., 2010; Wills, et al., 1999) and other previous studies examining *Abl* mutant alleles for *Drosophila* motor axon guidance defects). (G-H) Abl works with *Mical* to direct axon-axon

defasciculation/repulsion. **(G)** Utilizing a hypomorphic *Abl* mutant allele (*Abl<sup>l2</sup>*), reveals that decreasing the levels of Mical enhances the abnormal fasciculation of axons seen in *Abl* hypomorphic mutants. The graph represents the percentage (%) of ISNb axon guidance defects that are characteristic of increased axon-axon fasciculation (e.g., failure of ISNb axons to defasciculate from the main ISN nerve or stalling of ISNb axons [scored for the lack of innervation of both muscles 6/7 and 12/13]).  $n \geq 100$  hemisegments/genotype;  $\chi^2$  test; \*\*\*\* $p \leq 0.0001$ . *Mical<sup>+/-</sup>* = *Mical<sup>Df(3R)Swp2</sup>*, *Abl<sup>+/-</sup>* = *Abl<sup>l2</sup>*. **(H)** Decreasing the levels of *Abl* (*Abl<sup>+/-</sup>*) suppresses the ISNb axonal defasciculation defects seen with increasing *Mical* levels (neuronal specific *Mical* overexpression [*Mical<sup>+/+</sup>*; (Hung, et al., 2010)]). The graph represents the percentage (%) of ISNb axon guidance defects that are characteristic of increased axon-axon defasciculation (scored for the abnormal projection of ISNb axons, projecting into abnormal target fields, and presence of axons in abnormal areas; arrowheads).  $n \geq 95$  hemisegments/genotype;  $\chi^2$  test; \*\*\* $p \leq 0.001$ . *Abl<sup>+/-</sup>* = *Abl<sup>l/+</sup>*.

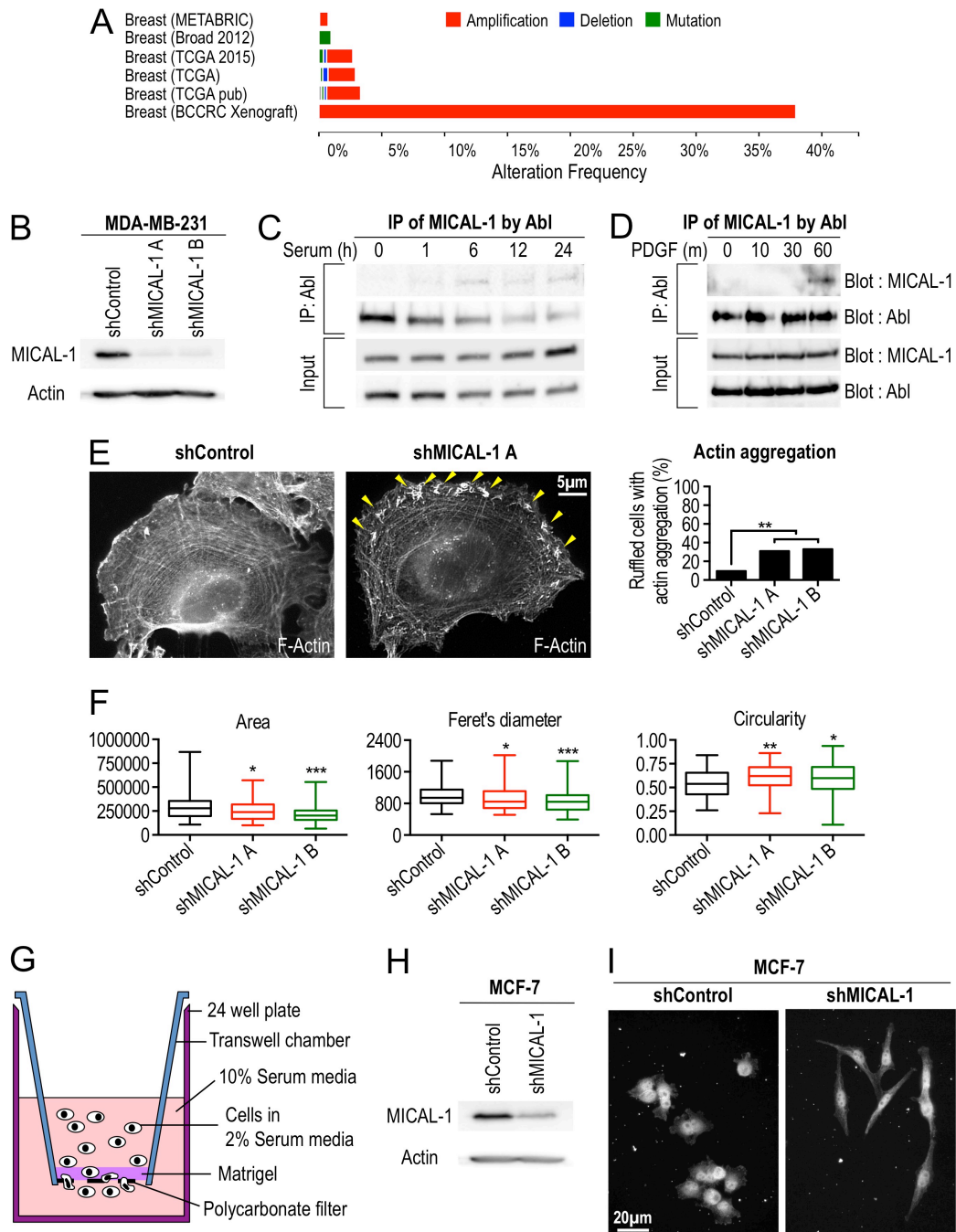
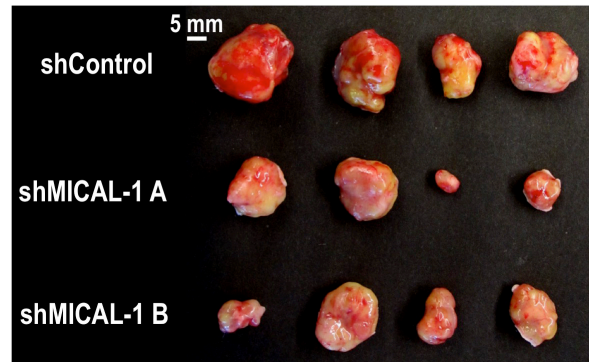


**Figure S6. MICAL-1 regulates breast cancer cell actin organization and morphology in vitro. Related to Figure 6.** (A) Small molecule tyrosine kinase inhibitors, including Gleevec (imatinib mesylate, STI571), are widely used to treat Abl-related cancers, but resistance to these inhibitors, including de novo point mutations within Abl tyrosine kinases, is one of the major hurdles to overcome in effective Abl-related cancer treatment. Thus, identification of other targets is needed for effective personalized therapy for Abl-related cancer patients. Summary of genomic alterations (red, amplification; blue, deletion; green, mutation) of MICAL-1 from 6 sequencing studies of the genomes of different isolated breast cancers. Note, that these various breast cancer samples show altered gene levels and mutations of MICAL-1, supporting a role for MICAL-1 in breast cancer. The data was obtained and modified from cBioPortal for Cancer Genomics ([www.cbioportal.org](http://www.cbioportal.org)). (B) Human MICAL-1 is expressed in MDA-MB-231 cells, a poorly differentiated, highly invasive breast cancer cell line (e.g., lane 1, staining with a MICAL-1 antibody). Using a lentivirus expressing an shRNA against human MICAL-1, we were also able to generate MDA-MB-231 cancer cell lines in which MICAL-1 was knocked down. The extent of the knockdown was determined by Western blotting using a MICAL-1 antibody and shows that the levels of MICAL-1 protein were substantially decreased by MICAL-1 shRNA (in two independent lines) compared to non-silencing control shRNA. Actin immunostaining was used to confirm that equal amounts of each sample were loaded. (C-D) Immunoprecipitation experiments using MDA-MB-231

cancer cells where both the IP and Input was blotted with MICAL-1 and Abl in both (C) and (D). (C) MICAL-1 associates with Abl in MDA-MB-231 cancer cells in response to growth factor serum stimulation. Cell lysates from serum (10 %) stimulated MDA-MB-231 breast cancer cells were immunoprecipitated with Abl antibodies and subjected to immunoblotting analysis with MICAL-1 antibodies. Note that the interaction becomes strongest beginning at 6hr after serum stimulation (top row as in D). Immunoblotting of total cell lysates with MICAL-1 antibodies and Abl antibodies was used to show the amounts of protein used for immunoprecipitation (as in D). (D) MICAL-1 associates with Abl in MDA-MB-231 cancer cells in response to PDGF application. Cell lysates from PDGF stimulated MDA-MB-231 breast cancer cells were immunoprecipitated with Abl antibodies and subjected to immunoblotting analysis with MICAL-1 antibodies. Note that the interaction becomes strongest beginning at 1hr after PDGF stimulation. Immunoblotting of total cell lysates with MICAL-1 antibodies and Abl antibodies was used to show the amounts of protein used for immunoprecipitation. These results indicate that Mical and Abl interactions are also controlled in cancer cells by growth factor/growth factor receptors. (E) Decreasing the levels of MICAL-1 in MDA-MB-231 cancer cells induces cell morphological changes including increased actin aggregation (yellow arrowheads) in membrane ruffles. F-actin was stained with phalloidin.  $n \geq 43$  cells/genotype;  $\chi^2$  test;  $**P \leq 0.01$ . (F) ShRNA-mediated knockdown of MICAL-1 in MDA-MB-231 breast cancer cells results in alterations to cell area, diameter, and circularity.  $n \geq 110$ ; Box and whiskers; t-test (compared with shControl);  $*P \leq 0.05$ ;  $**P \leq 0.01$ ;  $***P \leq 0.001$ . (G) Diagram outlining the experimental set-up of a matrigel invasion assay, which was used to examine the migratory/invasive properties of MDA-MB-231 breast cancer cells. See **Figure 6A**. (H) Human MICAL-1 is expressed in MCF-7 cells, a highly-differentiated, non-invasive, colony-forming breast cancer cell line (e.g., lane 1, staining with a MICAL-1 antibody). Using a lentivirus expressing an shRNA against human MICAL-1, we were also able to generate MCF-7 cancer cells in which MICAL-1 was knocked down. The extent of the knockdown was determined by Western blotting using a MICAL-1 antibody and shows that the levels of MICAL-1 protein were substantially decreased by MICAL-1 shRNA compared to non-silencing control shRNA. Actin immunostaining was used to confirm that equal amounts of each sample were loaded. (I) Decreasing the levels of MICAL-1 in MCF-7 cells induces cell morphological changes (compare to non-silencing control shRNA (shControl)).

A



B

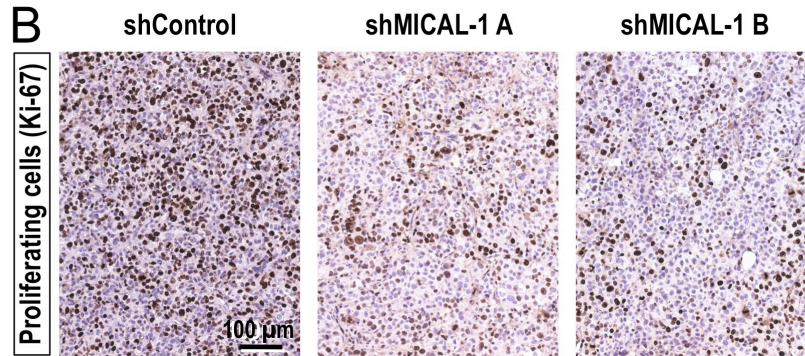


**Figure S7. Further analyses of MICAL-1 knockdown effects on xenograft tumor size and cancer cell proliferation in vivo. Related to Figure 6. (A)** Isolated MICAL-1 knockdown tumors dissected nine weeks following injection show a decreased size compared to controls. See also **Figure 6D** for analysis of data. **(B)** MICAL-1 knockdown tumors have less proliferating cells. Representative images showing proliferating cells by Ki-67 immunohistochemical staining. See also **Figure 6G** for analysis of data.